
Deep Learning and Hyperspectral Images Based Tomato Soluble Solids Content and Firmness Estimation

Yun Xiang¹, Qijun Chen¹, Zhongjin Su¹, Lu Zhang¹, Zuohui Chen¹, Guozhi Zhou², Zhuping Yao², Qi Xuan^{1,*} and Yuan Cheng^{2,*}

¹*Institute of Cyberspace Security, Zhejiang University of Technology, Hangzhou, China*

²*Institute of Vegetables, Zhejiang Academy of Agricultural Sciences, Hangzhou, China*

Correspondence*:

Qi Xuan, Yuan Cheng

xuanqi@zjut.edu.cn, Chengyuan1005@126.com

ABSTRACT

Cherry tomato (*Solanum lycopersicum*) is popular with consumers over the world due to its special flavor. Soluble solids content (SSC) and firmness are two key metrics for evaluating the product qualities. In this work, we develop non-destructive testing techniques for SSC and fruit firmness based on hyperspectral images and corresponding deep learning regression model. Hyperspectral reflectance images of over 200 tomato fruits are derived with spectrum ranging from 400 to 1000 nm. The acquired hyperspectral images are corrected and the spectral information are extracted. A novel one-dimensional(1D) convolutional ResNet (Con1dResNet) based regression model is proposed and compared with the state of art techniques. Experimental results show that, with relatively large number of samples our technique is 26.4% better than state of art technique for SSC and 33.7% for firmness. The results of this study indicate the application potential of hyperspectral imaging technique in the SSC and firmness detection, which provides a new option for non-destructive testing of cherry tomato fruit quality in the future.

Keywords: hyperspectral imaging, deep learning, cherry tomato, soluble solids content, One-dimensional Convolutional Neural Networks, firmness

1 INTRODUCTION

Tomato is a very popular fruit globally and its annual production reaches 186.82 million tons in 2020(FAO, 2021). Tomatoes contain rich nutrients such as lycopene, β -carotene and vitamins (Sainju et al., 2003; Gao et al., 2020) etc. To facilitate the tomato production, processing, and marketing, its grade and maturity needs to be evaluated. In general, soluble solids and firmness are two key indicators (Beckles, 2012). SSC can be used to grade tomato quality and the firmness can be used to determine fruit maturity (Peng and Lu, 2008). The existing measuring techniques relying upon chemistry reactions can derive the SSC value accurately. However, the destructive methods can not be applied in high volume measurements. Moreover, there are significant variations so that sampling can be inefficient and inaccurate(Li et al., 2013). Therefore,

in this work, we propose a hyperspectral imaging and deep learning based technique to measure tomato SSC and firmness nondestructively, accurately, and in high volume.

Spectroscopy is a widely used nondestructive testing method for fruit inspection. It includes various imaging techniques including visible, near infrared, terahertz spectroscopy, raman spectroscopy, and hyperspectral imaging etc. Visible and near infrared spectroscopy are rapid, convenient, and low cost. However, they are constrained by limited spectral band (Yin et al., 2019). Terahertz (THz) radiation has microwave and infrared properties and is able to penetrate and interact with many common materials, its equipments are very expensive (Afsah-Hejri et al., 2019). Raman spectroscopy is easy to operate, quick to measure, and contains rich information. However, its performance is inferior in terms of stability and sensitivity (Weng et al., 2019). Hyperspectral imaging technology can simultaneously detect the two-dimensional spatial information and 1D spectral information, therefore combine image and spectral characteristics (Adão et al., 2017). It can derive the overall spatial spectral information of cherry tomato and thus, is selected as the imaging method.

Hyperspectral imaging has been widely used for non-destructive testing in various fields, such as detection of plant disease stress (Lowe et al., 2017), industrial food packaging (Medus et al., 2021), medical image classification (Jeyaraj and Nadar, 2019), and horticultural products (Huang et al., 2017). Hyperspectral images are also effective for quality analysis of fruits. Rahman et al. (2017) use hyperspectral imaging to estimate metrics such as water content and PH readings. Zhou et al. (2020) use it to classify the maize seeds. Fan et al. (2015) use it to predict SSC and firmness in pears. They combine the competitive adaptive reweighted sampling and successive projection algorithm to select the variables as in partial least squares regression (PLSR). Rahman et al. (2018) fit sweetness and firmness of tomato. Lu et al. (2017) gives a review of the application of recent hyperspectral techniques. Therefore, hyperspectral imaging techniques can effectively measure or classify fruit and vegetable products.

The existing spectral analysis techniques typically require a regression model to fit the spectral data (Jiang and Chen, 2015), which have been widely used in areas such as food, petrochemical, and pharmaceutical fields (Chen et al., 2018). In general, various machine learning based algorithms are employed to build classification and regression models for hyperspectral images. Li et al. (2016) use PLSR to build a hyperspectral regression model to predict the water status of grapevines. Guo et al. (2016a) develop an SVM model to assess the maturity of strawberries. Abdulridha et al. (2019) combine hyperspectral imaging and KNN algorithm to differentiate ulcer-infected fruits. Ji et al. (2019) use the AdaBoost algorithm to recognize the rate of potato damage. The machine learning algorithms typically perform a filtering process on the spectral bands.

Deep learning models, e.g., convolutional neural network (CNN), can learn features automatically from a large amount of data (Guo et al., 2016b). It is widely used in medics (Esteva et al., 2019), industry (Hossain et al., 2018), agriculture (Kamilaris and Prenafeta-Boldú, 2018), object detection (Zou et al., 2019), and signal processing (Yu and Deng, 2010) etc. This technique is also used in building hyperspectral correction models for classification and prediction. Paoletti et al. (2019) summarize the application of deep learning for hyperspectral image classification and conclude that CNN based models are generally more effective due to their capacity to extract highly discriminatory features and leverage the spatial and spectral information. Qiu et al. (2018) demonstrate that CNN outperforms other machine learning methods for rice variety identification application. Kong et al. (2014) track activity of peroxidase in tomato hyperspectral images using genetic algorithm and extreme learning machine. Rahman et al. (2018) develop a regression model in 1000- 1550 nm hyperspectral images using PLSR method to estimate sweetness and firmness with R^2 of 0.672 and 0.548, respectively.

In this work, we propose a deep learning and hyperspectral imaging based technique to estimate the metrics inside cherry tomato. Specifically, we have made the following contributions.

1. We demonstrate the effectiveness of deep learning based techniques and propose such a model to estimate fruit SSC and firmness.
2. We explore the tradeoff between sample number and model accuracy.
3. We collect real-world field data and evaluate the performance of our technique.

The experimental results show that our technique is 26.4% better than the state of art technique in SSC estimation and 33.4% in firmness estimation.

2 MATERIALS AND METHODS

In this section, we describe the sample preparation, hyperspectral image acquisition and calibration, and the ground truth measurements for SSC and firmness methods. Specifically, we develop Con1dResNet, a deep learning and hyperspectral image based SSC and firmness estimation technique. Meanwhile, four comparing baseline techniques are also introduced.

2.1 Sample Preparation

The sample plant is a local mainstream cherry tomato (cultivar: Zheyangfen-1). The seeds first grow in the lab with tight environment control for one month. Then the seedlings are transplanted to the greenhouse of the Zhejiang academy of agricultural sciences, Hangzhou, China (east longitude 120°2', north latitude 30°27') on April 2nd (early spring), 2021. Field management is implemented following the standard commercial procedures. Cherry tomato fruits are harvested in June 2021. 200 fully mature fruits are collected from 50 different plants for hyperspectral image acquisition. Firmness and soluble solids content of each fruit is measured using portable firmness tester and hand-held refractometer after image acquisition, respectively.

2.1.1 Hyperspectral Image Acquisition

A hyperspectral imaging system is used to derive the hyperspectral images as shown in Fig.1. We use a push-broom hyperspectral camera (PIKA XC, Resonon Inc., Bozeman, MT, USA) mounted 20 cm above the tomato samples. The hyperspectral images are acquired with the spatial resolution of 50 pixels per mm^2 under artificial lighting (four 15W 12 V light bulbs with two on either side of the lens). The main specifications of the hyperspectral camera were: interface, Firewire (IEEE 1394b), digital output (14 bit), and angular field of view of 7 degrees. The objective lens had a 17 mm focal length (maximum aperture of F1.4), optimized for the hyperspectral. We acquire reflectance data in 462 spectral bands from 386 to 1004 nm with a spectral resolution of 1.3 nm. Due to the convex surface of the samples, the uneven reflection creates a highlighted region near the vertical axial as shown in Fig.2A. Thus, we use ENVI5.3 (ITT, Visual Information Solutions, Boulder, CO, USA) (Su et al., 2021) to avoid the highlight region and extract the reflection value for each band from the region of interest (Xue, 2010; Fu et al., 2021) (Fig.2B).

2.1.2 Hyperspectral Image Calibration

In reflectance calibration, the acquired hyperspectral image needs to be calibrated for the background spectral response of the instrument and the thermal dark current of the camera. The spectral data collected from the CCD device contains only the detector signal intensity value (Elmasry et al., 2012). Therefore, it is required to convert the raw data to reflectance or absorptivity values by comparing to the spectra of

standard reference substances (Burger and Geladi, 2005) as shown in Fig.3. The reflectance can be derived using the following equation.

$$R_c = \frac{R_{ori} - R_{dark}}{R_{white} - R_{dark}},$$

where R_c is the corrected hyperspectral reflectance, R_{ori} is the original reflection value extracted from ENVI5.3, R_{dark} is the dark environment hyperspectral image reflection value, which is acquired using an opaque lens cap covering the hyperspectral lens, and R_{white} is the reflection value of a piece of white Teflon (100% reflectance, K-Mac Plastics, MI, USA).

2.1.3 Baseline Measurement

The baseline firmness and SSC of cherry tomatoes are measured in the lab. For the firmness measurement, the cherry tomatoes are fixed on a portable firmness measurement equipment (GY-4, Zhejiang Top Cloud-Agri Technology Co., Ltd, China). The equipment is zero-calibrated. Starting from the contact of the probe with the cherry tomato surface, the 10 mm downward pressure is considered as the firmness value.

SSC measurements follow the firmness measurements. Cherry tomatoes are cut along the vertical axis and wrapped using a gauze. Then they are squeezed manually to force out the solution. About one milliliter tomato solution is placed on the prism of a portable digital refractometer (PAL-1, ATAGO CHINA Guangzhou Co., Ltd, China) to derive the baseline SSC readings. Each cherry tomato sample solution is measured for 3 times and the results are averaged to reduce the effect of random environment events.

2.2 Image Processing Models

2.2.1 Deep Learning Model

Deep learning models are widely used in medical image processings (Kiranyaz et al., 2015). However, in this work, it is required to build appropriate regression models. In general, we propose the Con1dResNet model to estimate the tomato SSC and firmness.

ResNet (He et al., 2016), a popular model for image classification, can solve the degradation problem of deep networks. Thus, ResNet34 is implemented as the baseline network structure, and the original convolutional layer is reconstructed to be one-dimensional, accordingly. We use the Adam optimizer and mean squared error loss function. We change the number of categories output by the last fully connected layer to one so that the network directly outputs the estimated values of SSC and firmness.

The specific network structure is shown in Fig.4. In the figure, the input is the reflectance values of the processed 462 spectral bands. There are five main blocks. The first block consists of a 1D convolution layer and a maximum pool layer, and then continues through a dropout layer with parameter 0.5. The second blockX contains 3 residuals module. The third blockX contains 1 downsampled module and 3 residuals module. The fourth blockX goes through 1 downsampled module and 5 residuals module before a dropout layer with parameter 0.5, and then continues through 3 residuals module. The fifth block consists of a mean pool layer and linear output layer. The number of convolution filters doubles as the block goes deeper (starting with 32 and ending with 128). All convolutional layers have a kernel size of 3 and a step size of 3. By connecting the convolutional layers together, deeper layers can be connected to a larger portion of the original input. Thus, different layers see the original input and learning ability at different levels. The last deeper layer outputs the SSC estimation, which converge to the ground truth value under the approximation of the MSE loss function.

2.2.2 Machine Learning Models

The existing image feature extraction methods are mostly based on machine learning models. In this work, we select four widely-used models as references to our deep learning based technique.

2.2.2.1 SVR

Support Vector Regression(SVR) (Castro-Neto et al., 2009) is a variant of the support vector machines (SVM) technique (Burges, 1998). SVR is widely used in spectral data analysis for its linear and nonlinear processing ability. SVR maps the data to a high-dimensional space and constructs a hyperplane to minimize the distance to the farthest sample point. In SVR, the selection of an appropriate kernel function is crucial. We implement an SVR model with Radial basis function (RBF), which can process nonlinear data effectively.

2.2.2.2 KNNR

K-Nearest Neighbors Regression(KNNR) (Yao and Ruzzo, 2006) is a nonparametric method that approximates the association between independent variables and continuous outcomes. Intuitively, it averages observations in the same neighborhood. The size of the neighborhood can be set using cross-validation to minimize the mean squared error. The number of neighborhoods in this work is set to 5.

2.2.2.3 AdaBoostR

Adaptive Boosting Regression(AdaBoostR) (Freund et al., 1999) is an iterative boosting algorithm. An AdaBoost regressor is a meta-estimator. It first fits a regression measure on the original dataset, then fits other copies of the regression measure on the same dataset. The weights of the instances are adjusted according to the error of the current estimation. The learning rate is the weight reduction factor of each weak learner. In this work, we set the learning rate to 0.8 and the number of iterations to 60.

2.2.2.4 PLSR

Partial Least Squares Regression(PLSR) (Wold et al., 2001) combines the advantages of multiple linear regression and principal component analysis (Jolliffe, 2005). The principal component pairs are derived by calculating the correlation coefficient matrix. Several spectral bands with relatively highest contribution values are selected to reduce noise. In this work, we use grid search to determine the principal component and train the network for 50,000 iterations.

3 RESULTS

In this section, we evaluate our techniques in SSC and firmness estimation.

3.1 Data Set Processing

The processed cherry tomato samples and the corresponding hyperspectral images are divided into training set, validation set, and test set with ratio of 7:1:2, respectively. We use varying data set size, with a small set of 50 samples and a large set of 200 samples. Fig.5A shows the reflectance spectra of 200 cherry tomato samples at 386-1004 nm. The spectral trends are similar for each sample since the reflection substances are the same. The cherry tomatoes have a strong absorption band at 400-550 nm due to the presence of carotenoids in ripe tomatoes(Ecarnot et al., 2013).The reflectance data are then processed using multiple scattering correction(MSC). As shown in Fig.5B, it can effectively reduce the noise and hence,

smooth the curve. Finally, we use second order differentiation method (Ichige et al., 2006) to process the smoothed reflectance data and discover clear peaks at locations of 580-590 nm, 680-690 nm, and 970-980 nm, as shown in Fig.5C. The three peaks are likely to be attributed to the combined effect of the second overtone of OH key, water, and tomato surface color(Li et al., 2013; Qiu et al., 2018). Therefore, by proper processing, the variations in the spectral curves can reveal certain hidden information, such as SSC and water.

3.2 Analysis

Table 1 summarizes the distribution characteristics of SSC and firmness in different stages. The SSC and firmness measurements for the 50 and 200 samples are close to normally distributed around the mean values of 9.11° Brix, 9.04 N/cm² and 8.72° Brix, 8.85 N/cm², standard deviations (SD) of 0.76, 1.35, and 0.66, 1.23, respectively.

3.3 SSC Estimation Result

Four machine learning models are implemented and compared with our proposed Con1dResNet network. We use R^2 and MSE as the evaluation metrics. They are calculated using the following equations.

$$R^2 = 1 - \frac{\sum_i (\hat{y}_i - y_i)^2}{\sum_i (\bar{y}_i - y_i)^2}$$

$$MSE = \frac{1}{m} \sum_{i=1}^m (y_i - \hat{y}_i)^2$$

where \hat{y}_i is the estimated value, y_i is the ground true value, and \bar{y}_i is the mean value. The optimal R^2 and MSE values are 1 and 0, respectively.

The algorithms are trained and run on a platform with an I7-8750H CPU and a 1060 GPU. They are programmed using python and tensorflow etc. The data sets are divided as described in Table 1. The processed spectral data are used in the machine learning models while the raw spectral data are used in the Con1dResNet network. Since our deep learning model Con1dResNet can extract low to high dimensional features automatically, we use the original spectral data instead. We set Relu as the activation function, Adam as the optimizer, MSE as the loss function, the number of iterations to 50, and the batch size to 16. After 50 iterations of training, the loss decreases from 72.86 at the beginning to 0.01, indicating a convergence for the algorithm.

The experimental results are shown in Fig.6 and Table 2. In general, the second-order differential processing outperforms MSC. However, since the SVR and KNNR models lack the ability of data dimensionality reduction, the noise caused by unwanted reflectance cannot be removed. When the data size increases, the amount of interference also rises. Thus, the R^2 value decreases as the data size increases. As expected, they have the worst performance with R^2 less than 0.4. For AdaBoostR, PLSR, and Con1dResNet models, R^2 values increase with increasing data sets size. For a relatively smaller data size, the PLSR model achieves the best performance, with R^2 of 0.577 and MSE of 0.055. As the data size increases, the performance of the Con1dResNet model is improved significantly, with R^2 increasing from 0.498 to 0.901 (26.4% better than the second best) and MSE decreasing from 0.065 to 0.018.

3.4 Firmness Estimation Result

The same experimental setup is employed for firmness detection. As shown in Table.3 and Fig.7, when MSC is employed for AdaBoost and PLSR, their R^2 values can be significantly improved (Wang et al., 2014). Therefore, we choose MSC as the preprocessing method for AdaBoost and PLSR, and second-order difference as the preprocessing method for SVR and KNNR. Although the method developed in this study has some advantages in data feature extraction compared with other methods, R^2 is still only 0.53, which does not achieve the accurate estimation standard. The R^2 of SVR and KNNR models is negative, which indicates the estimation accuracy is lower than the mean value.

4 DISCUSSION

The tomato flavor is important. SSC, which mainly consists of soluble sugars, can reflect the sweetness of cherry tomato. Hyperspectral imaging has been considered an effective technique for fruit SSC and firmness evaluation (Fan et al., 2015; Lu, 2004). In this work, we discover a great estimation result for SSC estimation, while an inferior result for firmness.

In general, the extracted spectral features (Guo et al., 2016a) can derive excellent estimation results for large sample size. In that case, the deep learning based model performs significantly better than other machine learning based techniques since it can map the solution space to higher dimensions. For the PLSR (Wold et al., 2001) model, it includes a principal component analysis component, which performs screening of band contribution values before training, and then selects 5-15 bands with relatively large contribution rates for regression. Thus, it can remove the influence of interfering bands (He et al., 2019) and have more interference-free learning materials when the data size is large. Therefore, it can boost R^2 when the data size increases. Combined with the removal of the invalid interference bands, the PLSR model becomes the state of art machine learning model. However, as the number of sample size increases, the value of Con1dResNet model starts to gradually outperform the PLSR model due to the feature extraction ability of deep learning models. The experimental results demonstrate that Con1dResNet can significantly outperform the existing machine learning based techniques, with R^2 of 0.901 and MSE of 0.018. We believe that the experimental results of this work are also indicative for other horticultural crops.

For the hyperspectral images based tomato firmness, although it is reported that hyperspectral images can estimate fruit firmness (Fan et al., 2015; Lu, 2004), our experimental results suggest otherwise. Rahman et al. (2018) use PLSR to estimate tomato firmness using hyperspectral images in the 1000-1550 nm wavebands, and derive R^2 value of 0.6724. It is a little higher than our experiment due to the differences in the used hyperspectral wavebands and the experimental environments. Therefore, in future work, for the estimation of firmness, we should explore a wider range of hyperspectral image wavebands, optimize the parameters for the firmness experiments, and improve the overall estimation accuracy.

5 CONCLUSION

In this work, we propose Con1dResNet, a deep learning based technique, to estimate the SSC and firmness of cherry tomatoes using hyperspectral images. With sufficient sample size, it can achieve better results than traditional machine learning methods. For SSC estimation, its R^2 value is 0.901, which is 26.4% higher than PLSR, while its MSE is 0.018, which is 0.046 lower than PLSR. For Firmness estimation, its R^2 value is 0.532, which is still 33.7% better than PLSR. The results indicate that hyperspectral imaging

combined with deep learning can significantly improve the cherry tomato SSC and firmness estimation accuracies.

DATA AVAILABILITY STATEMENT

The raw data supporting the conclusions of this article will be made available by the authors, without undue reservation.

FUNDING

This work was supported by Provincial Key Research and Development Program of Zhejiang (2021C02052).

AUTHOR CONTRIBUTIONS

YX, QC, YC, QX and ZS performed a conceptual, formal analysis of the study. QC, YX, ZC, and YC wrote the manuscript. YX, YC, QC, LZ, GZ, ZY, and QX designed the experiment. QC, LZ and ZS wrote the experimental code. YX, and QX verified the experimental results. All authors contributed to the article and reviewed the manuscript.

REFERENCES

- Abdulridha, J., Batuman, O., and Ampatzidis, Y. (2019). Uav-based remote sensing technique to detect citrus canker disease utilizing hyperspectral imaging and machine learning. *Remote Sensing* 11, 1373. Doi: 10.3390/rs11111373
- Adão, T., Hruška, J., Pádua, L., Bessa, J., Peres, E., Morais, R., et al. (2017). Hyperspectral imaging: A review on uav-based sensors, data processing and applications for agriculture and forestry. *Remote Sensing* 9, 1110. Doi: 10.3390/rs9111110
- Afsah-Hejri, L., Hajeb, P., Ara, P., and Ehsani, R. J. (2019). A comprehensive review on food applications of terahertz spectroscopy and imaging. *Comprehensive reviews in food science and food safety* 18, 1563–1621. Doi: 10.1111/1541-4337.12490
- Beckles, D. M. (2012). Factors affecting the postharvest soluble solids and sugar content of tomato (*solanum lycopersicum* l.) fruit. *Postharvest Biology and Technology* 63, 129–140. Doi: 10.1016/j.postharvbio.2011.05.016
- Burger, J. and Geladi, P. (2005). Hyperspectral nir image regression part i: calibration and correction. *Journal of Chemometrics: A Journal of the Chemometrics Society* 19, 355–363. Doi: 10.1002/cem.938
- Burges, C. J. (1998). A tutorial on support vector machines for pattern recognition. *Data mining and knowledge discovery* 2, 121–167. Doi: 10.1023/A:1009715923555
- Castro-Neto, M., Jeong, Y.-S., Jeong, M.-K., and Han, L. D. (2009). Online-svr for short-term traffic flow prediction under typical and atypical traffic conditions. *Expert systems with applications* 36, 6164–6173. Doi: 10.1016/j.eswa.2008.07.069
- Chen, Q., Chen, M., Liu, Y., Wu, J., Wang, X., Ouyang, Q., et al. (2018). Application of ft-nir spectroscopy for simultaneous estimation of taste quality and taste-related compounds content of black tea. *Journal of food science and technology* 55, 4363–4368. Doi: 10.1007/s13197-018-3353-1
- Du, X., Cai, Y., Wang, S., and Zhang, L. (2016). Overview of deep learning. In *2016 31st Youth Academic Annual Conference of Chinese Association of Automation (YAC) (IEEE)*, 159–164. Doi: 10.1109/YAC.2016.7804882

- Ecarnot, M., Bączyk, P., Tessarotto, L., and Chervin, C. (2013). Rapid phenotyping of the tomato fruit model, micro-tom, with a portable vis–nir spectrometer. *Plant physiology and biochemistry* 70, 159–163. Doi: 10.1016/j.plaphy.2013.05.0198
- Elmasry, G., Kamruzzaman, M., Sun, D.-W., and Allen, P. (2012). Principles and applications of hyperspectral imaging in quality evaluation of agro-food products: a review. *Critical reviews in food science and nutrition* 52, 999–1023. Doi: 10.1080/10408398.2010.543495
- Esteva, A., Robicquet, A., Ramsundar, B., Kuleshov, V., DePristo, M., Chou, K., et al. (2019). A guide to deep learning in healthcare. *Nature medicine* 25, 24–29. Doi: 10.1038/s41591-018-0316-z
- Fan, S., Huang, W., Guo, Z., Zhang, B., and Zhao, C. (2015). Prediction of soluble solids content and firmness of pears using hyperspectral reflectance imaging. *Food analytical methods* 8, 1936–1946. Doi: 10.1007/s12161-014-0079-1
- [Dataset] FAO (2021). Tomato growth volume. <https://www.fao.org/faostat/en/#data/QCL/visualize>. Accessed December 27, 2021
- Freund, Y., Schapire, R., and Abe, N. (1999). A short introduction to boosting. *Journal-Japanese Society For Artificial Intelligence* 14, 1612
- Fu, D., Zhou, J., Scaboo, A. M., and Niu, X. (2021). Nondestructive phenotyping fatty acid trait of single soybean seeds using reflective hyperspectral imagery. *Journal of Food Process Engineering*, e13759 Doi: 10.1111/jfpe.13759
- Gao, Y.-F., Liu, J.-K., Yang, F.-M., Zhang, G.-Y., Wang, D., Zhang, L., et al. (2020). The wrky transcription factor wrky8 promotes resistance to pathogen infection and mediates drought and salt stress tolerance in solanum lycopersicum. *Physiologia plantarum* 168, 98–117. Doi: 10.1111/pp1.12978
- Guo, C., Liu, F., Kong, W., He, Y., Lou, B., et al. (2016a). Hyperspectral imaging analysis for ripeness evaluation of strawberry with support vector machine. *Journal of Food Engineering* 179, 11–18. Doi: 10.1016/j.jfoodeng.2016.01.002
- Guo, Y., Liu, Y., Oerlemans, A., Lao, S., Wu, S., and Lew, M. S. (2016b). Deep learning for visual understanding: A review. *Neurocomputing* 187, 27–48. Doi: 10.1016/j.neucom.2015.09.116
- He, K., Zhang, X., Ren, S., and Sun, J. (2016). Identity mappings in deep residual networks. In *European conference on computer vision* (Springer), 630–645
- He, Y., Zhao, Y., Zhang, C., Sun, C., and Li, X. (2019). Determination of β -carotene and lutein in green tea using fourier transform infrared spectroscopy. *Transactions of the ASABE* 62, 75–81. Doi: 10.13031/trans.12839
- Hossain, M. S., Al-Hammadi, M., and Muhammad, G. (2018). Automatic fruit classification using deep learning for industrial applications. *IEEE Transactions on Industrial Informatics* 15, 1027–1034. Doi: 10.1109/TII.2018.2875149
- Huang, Y., Lu, R., and Chen, K. (2017). Development of a multichannel hyperspectral imaging probe for property and quality assessment of horticultural products. *Postharvest Biology and Technology* 133, 88–97. Doi: 10.1016/j.postharvbio.2017.07.009
- Ichige, K., Ishikawa, Y., and Arai, H. (2006). Accurate direction-of-arrival estimation using second-order differential of music spectrum. In *2006 International Symposium on Intelligent Signal Processing and Communications* (IEEE), 995–998. Doi: 10.1109/ISPACS.2006.364805
- Jeyaraj, P. R. and Nadar, E. R. S. (2019). Computer-assisted medical image classification for early diagnosis of oral cancer employing deep learning algorithm. *Journal of cancer research and clinical oncology* 145, 829–837. Doi: 10.1007/s00432-018-02834-7

- Ji, Y., Sun, L., Li, Y., and Ye, D. (2019). Detection of bruised potatoes using hyperspectral imaging technique based on discrete wavelet transform. *Infrared Physics & Technology* 103, 103054. Doi: 10.1016/j.infrared.2019.103054
- Jiang, H. and Chen, Q. (2015). Chemometric models for the quantitative descriptive sensory properties of green tea (*Camellia sinensis* L.) using Fourier transform near infrared (FT-NIR) spectroscopy. *Food Analytical Methods* 8, 954–962. Doi: 10.1007/s12161-014-9978-4
- Jolliffe, I. (2005). Principal component analysis. *Encyclopedia of statistics in behavioral science* Doi: 10.1002/0470013192.bsa501
- Kamilaris, A. and Prenafeta-Boldú, F. X. (2018). Deep learning in agriculture: A survey. *Computers and electronics in agriculture* 147, 70–90. Doi: 10.1016/j.compag.2018.02.016
- Kiranyaz, S., Ince, T., Hamila, R., and Gabbouj, M. (2015). Convolutional neural networks for patient-specific ECG classification. In *2015 37th Annual International Conference of the IEEE Engineering in Medicine and Biology Society (EMBC) (IEEE)*, 2608–2611. Doi: 10.1109/EMBC.2015.7318926
- Kong, W., Liu, F., Zhang, C., Bao, Y., Yu, J., and He, Y. (2014). Fast detection of peroxidase (POD) activity in tomato leaves which infected with *Botrytis cinerea* using hyperspectral imaging. *Spectrochimica Acta Part A: Molecular and Biomolecular Spectroscopy* 118, 498–502. Doi: 10.1016/j.saa.2013.09.009
- Li, J., Huang, W., Zhao, C., and Zhang, B. (2013). A comparative study for the quantitative determination of soluble solids content, pH and firmness of pears by vis/NIR spectroscopy. *Journal of Food Engineering* 116, 324–332. Doi: 10.1016/j.jfoodeng.2012.11.007
- Li, J., Tian, X., Huang, W., Zhang, B., and Fan, S. (2016). Application of long-wave near infrared hyperspectral imaging for measurement of soluble solid content (SSC) in pear. *Food Analytical Methods* 9, 3087–3098. Doi: 10.1007/s12161-016-0498-2
- Lowe, A., Harrison, N., and French, A. P. (2017). Hyperspectral image analysis techniques for the detection and classification of the early onset of plant disease and stress. *Plant methods* 13, 1–12. Doi: 10.1186/s13007-017-0233-z
- Lu, R. (2004). Multispectral imaging for predicting firmness and soluble solids content of apple fruit. *Postharvest Biology and Technology* 31, 147–157. Doi: 10.1016/j.postharvbio.2003.08.006
- Lu, Y., Huang, Y., and Lu, R. (2017). Innovative hyperspectral imaging-based techniques for quality evaluation of fruits and vegetables: A review. *Applied Sciences* 7, 189. Doi: 10.3390/app7020189
- Medus, L. D., Saban, M., Francés-Víllora, J. V., Bataller-Mompeán, M., and Rosado-Muñoz, A. (2021). Hyperspectral image classification using CNN: Application to industrial food packaging. *Food Control* 125, 107962. Doi: 10.1016/j.foodcont.2021.107962
- Paoletti, M., Haut, J., Plaza, J., and Plaza, A. (2019). Deep learning classifiers for hyperspectral imaging: A review. *ISPRS Journal of Photogrammetry and Remote Sensing* 158, 279–317. Doi: 10.1016/j.isprsjprs.2019.09.006
- Peng, Y. and Lu, R. (2008). Analysis of spatially resolved hyperspectral scattering images for assessing apple fruit firmness and soluble solids content. *Postharvest Biology and Technology* 48, 52–62. Doi: 10.1016/j.postharvbio.2007.09.019
- Qiu, Z., Chen, J., Zhao, Y., Zhu, S., He, Y., and Zhang, C. (2018). Variety identification of single rice seed using hyperspectral imaging combined with convolutional neural network. *Applied Sciences* 8, 212. Doi: 10.3390/app8020212
- Rahman, A., Kandpal, L. M., Lohumi, S., Kim, M. S., Lee, H., Mo, C., et al. (2017). Nondestructive estimation of moisture content, pH and soluble solid contents in intact tomatoes using hyperspectral imaging. *Applied Sciences* 7, 109. Doi: 10.3390/app7010109

- Rahman, A., Park, E., Bae, H., and Cho, B.-K. (2018). Hyperspectral imaging technique to evaluate the firmness and the sweetness index of tomatoes. *Korean Journal of Agricultural Science* 45, 823–837. Doi: 10.7744/kjoas.20180075
- Sainju, U. M., Dris, R., and Singh, B. (2003). Mineral nutrition of tomato. *Food, Agriculture & Environment* 1, 176–183
- Su, Z., Zhang, C., Yan, T., Zhu, J., Zeng, Y., Lu, X., et al. (2021). Application of hyperspectral imaging for maturity and soluble solids content determination of strawberry with deep learning approaches. *Frontiers in plant science*, 1897 Doi: 10.3389/fpls.2021.736334
- Wang, D.-M., Ji, J.-M., and Gao, H.-Z. (2014). The effect of msc spectral pretreatment regions on near infrared spectroscopy calibration results. *Guang pu xue yu Guang pu fen xi= Guang pu* 34, 2387–2390
- Weng, S., Zhu, W., Zhang, X., Yuan, H., Zheng, L., Zhao, J., et al. (2019). Recent advances in raman technology with applications in agriculture, food and biosystems: A review. *Artificial Intelligence in Agriculture* 3, 1–10. Doi: 10.1016/j.aiia.2019.11.001
- Wold, S., Sjöström, M., and Eriksson, L. (2001). PLS-regression: a basic tool of chemometrics. *Chemometrics and intelligent laboratory systems* 58, 109–130. Doi: 10.1016/S0169-7439(01)00155-1
- Xue, L. (2010). Application of idl and envi redevelopment in hyperspectral image preprocessing. In *International Conference on Computer and Computing Technologies in Agriculture* (Springer), 403–409
- Yao, Z. and Ruzzo, W. L. (2006). A regression-based k nearest neighbor algorithm for gene function prediction from heterogeneous data. In *BMC bioinformatics* (BioMed Central), vol. 7, 1–11. Doi: 10.1186/1471-2105-7-S1-S11
- Yin, L., Zhou, J., Chen, D., Han, T., Zheng, B., Younis, A., et al. (2019). A review of the application of near-infrared spectroscopy to rare traditional chinese medicine. *Spectrochimica Acta Part A: Molecular and Biomolecular Spectroscopy* 221, 117208. Doi: 10.1016/j.saa.2019.117208
- Yu, D. and Deng, L. (2010). Deep learning and its applications to signal and information processing [exploratory dsp]. *IEEE Signal Processing Magazine* 28, 145–154. Doi: 10.1109/MSP.2010.939038
- Zhou, Q., Huang, W., Fan, S., Zhao, F., Liang, D., and Tian, X. (2020). Non-destructive discrimination of the variety of sweet maize seeds based on hyperspectral image coupled with wavelength selection algorithm. *Infrared Physics & Technology* 109, 103418. Doi: 10.1016/j.infrared.2020.103418
- Zou, Z., Shi, Z., Guo, Y., and Ye, J. (2019). Object detection in 20 years: A survey. *arXiv preprint arXiv:1905.05055*

FIGURE CAPTIONS

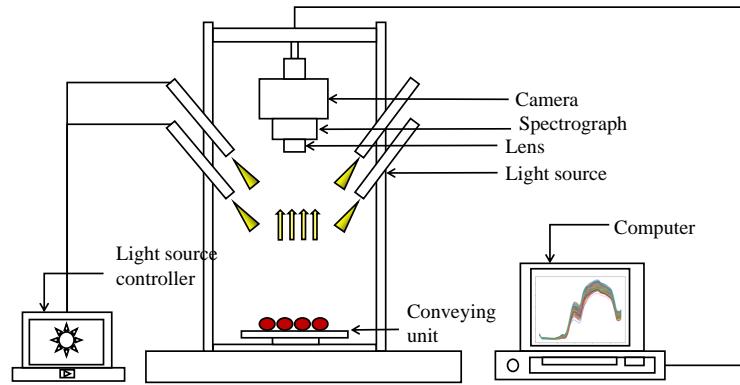


Figure 1. Schematic of the hyperspectral imaging system for acquiring spectral scattering images from cherry tomatoes

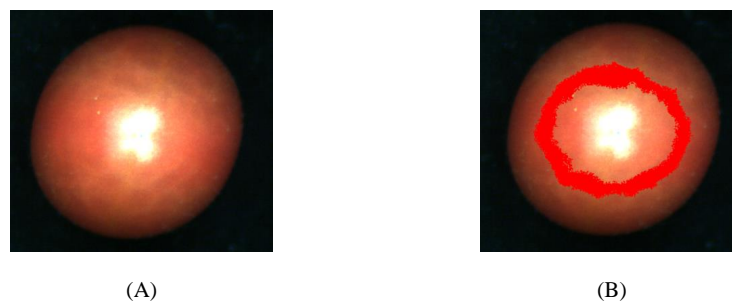


Figure 2. (A) ENVI original hyperspectral image, (B) area map of ROI acquired by ENVI

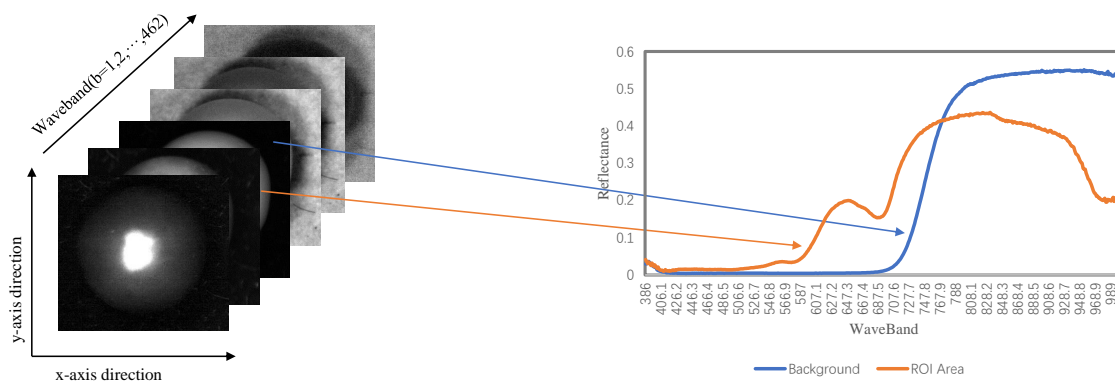


Figure 3. Schematic diagram of the structure and data of the corrected hyperspectral image: spatial axis x, y and wavebands

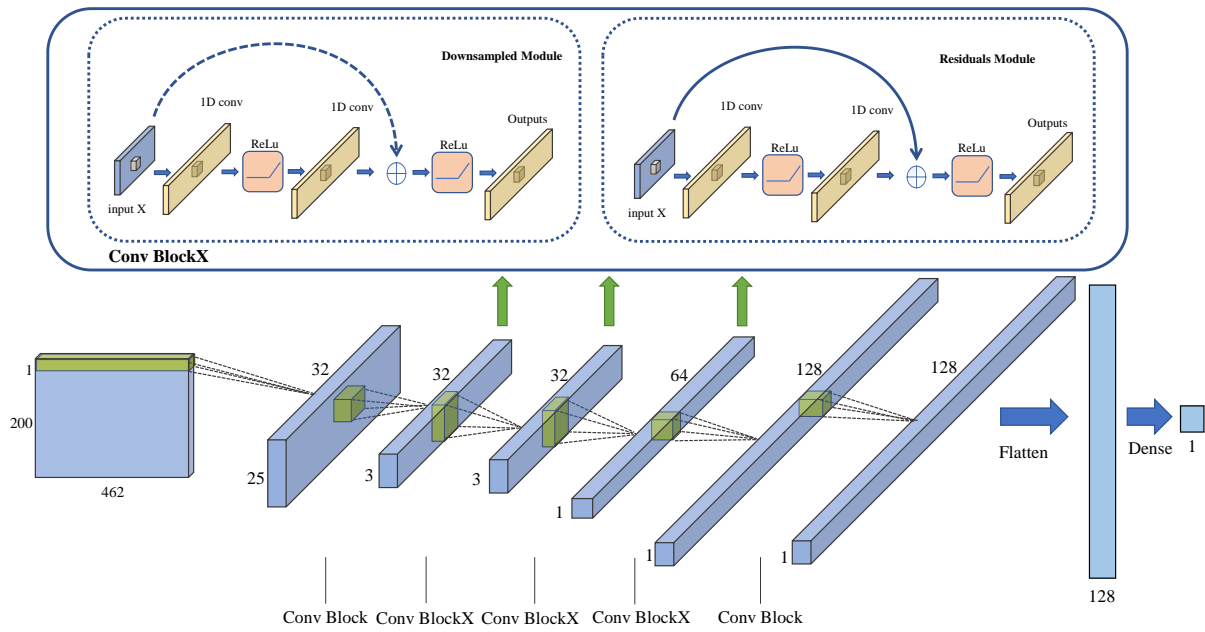


Figure 4. Con1dResNet network structure schematic

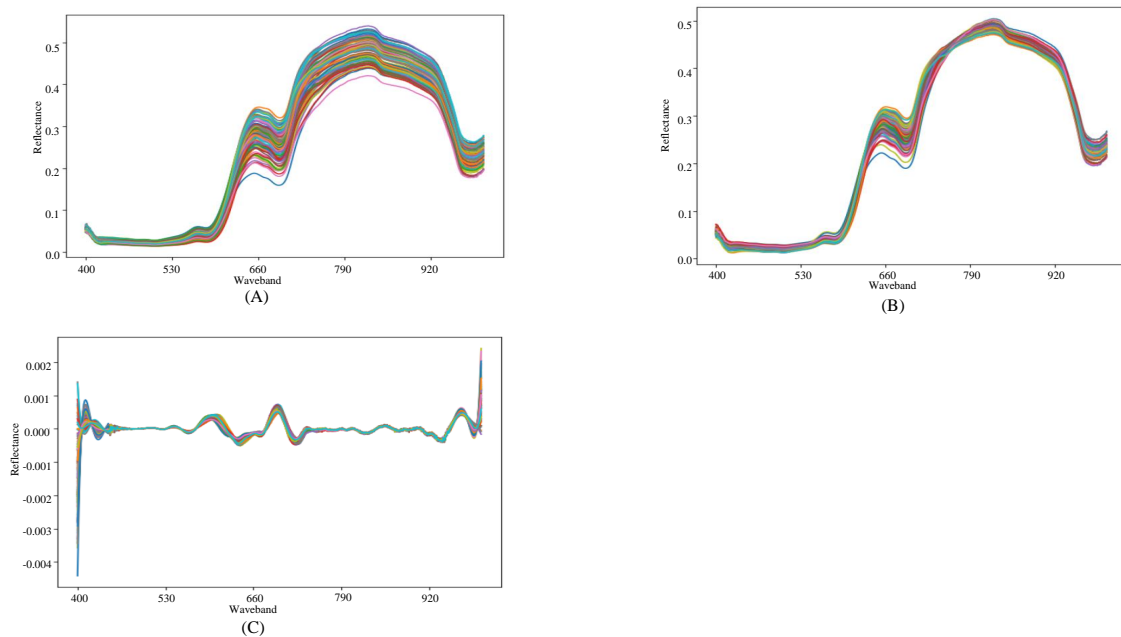


Figure 5. (A) Corrected spectral reflectance map, (B) MSC preprocessing, (C) Second-order differential preprocessing

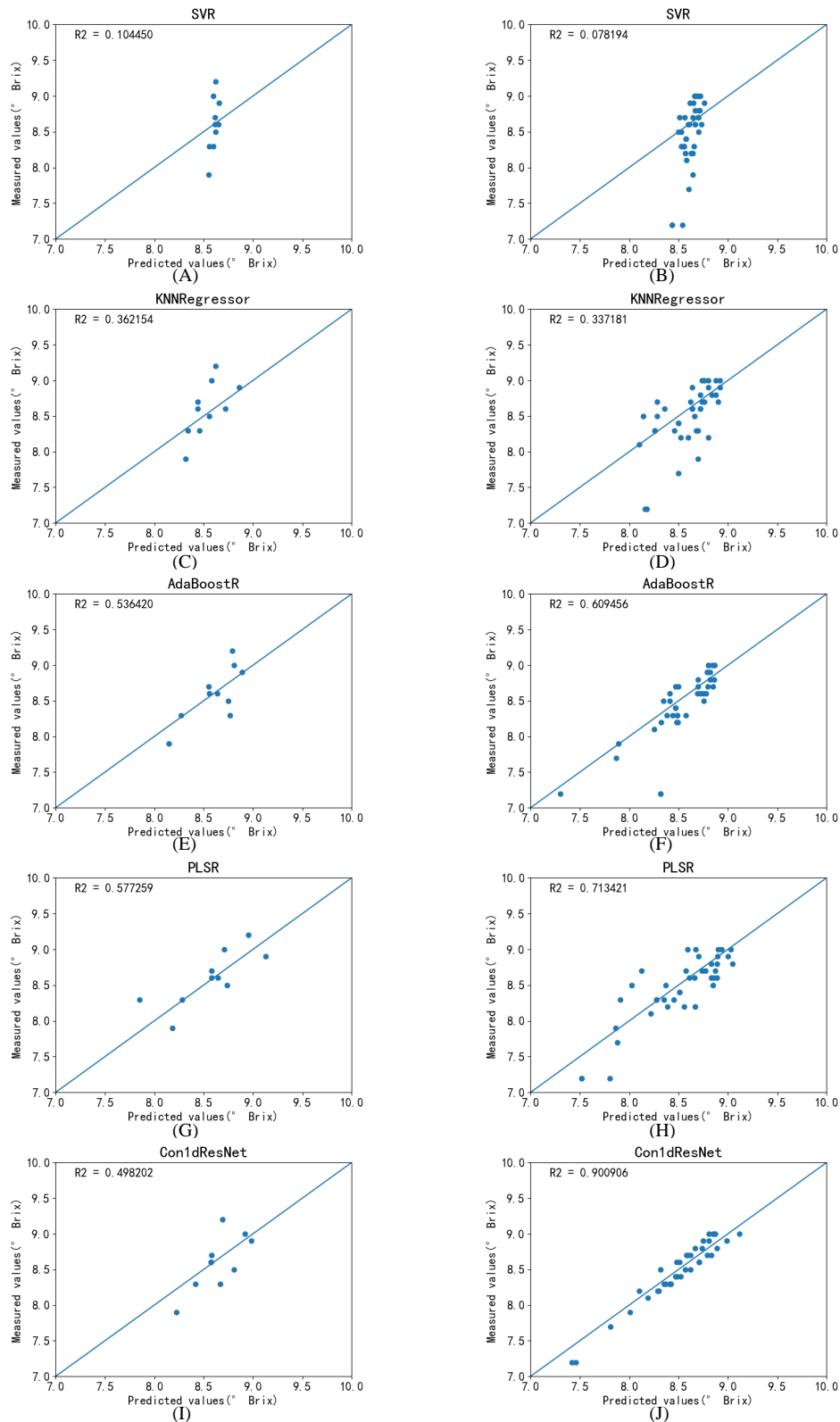


Figure 6. SS-C estimation results for each model. (A) SVR estimation results on small sample data, (B) SVR estimation results on large sample data, (C) KNNR estimation results on small sample data, (D) KNNR estimation results on large sample data, (E) AdaBoostR estimation results on small sample data, (F) AdaBoostR estimation results on large sample data, (G) PLSR estimation results on small sample data, (H) PLSR estimation results on large sample data, (I) Con1dResNet estimation results on small sample data, (J) Con1dResNet estimation results on large sample data

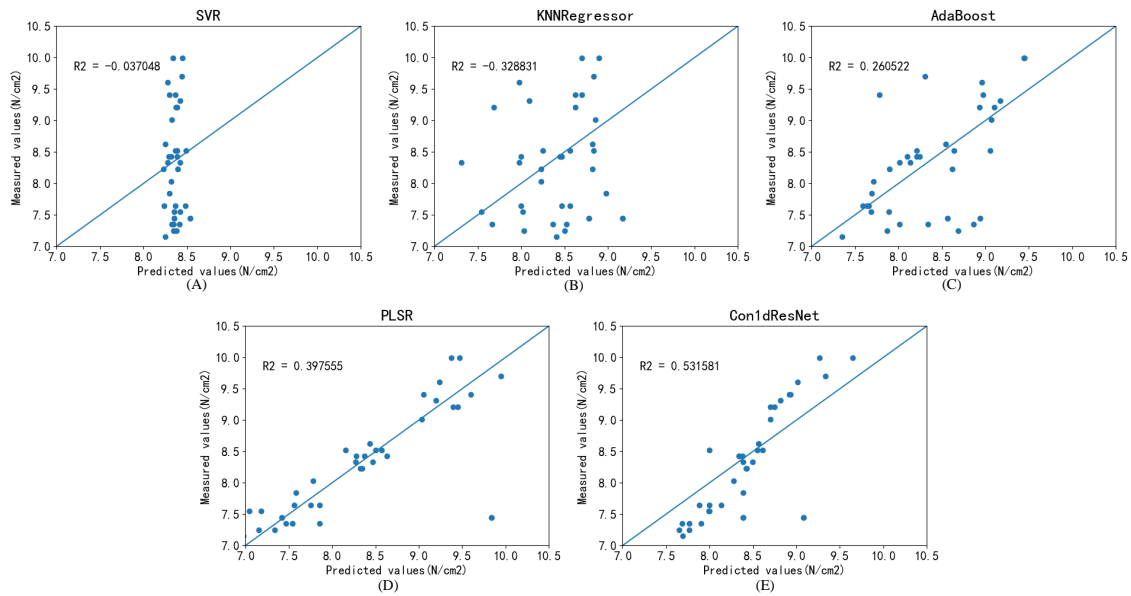


Figure 7. Estimation results of firmness for each model on a large sample dataset

Table 1. Cherry tomato SSC and firmness dataset partitioning

Sample Size	Dataset	SSC(° Brix)				firmness(N/cm2)			
		MAX	MIN	MEAN	STD	MAX	MIN	MEAN	STD
Small	Total(50)	10.800	8.000	9.114	0.726	12.642	5.978	9.038	1.351
	Train Set(35)	10.800	8.000	9.129	0.760	12.642	5.978	8.747	1.324
	Val Set(5)	10.400	8.700	9.320	0.779	9.800	8.624	9.153	0.488
	Test Set(10)	9.200	7.900	8.600	0.380	12.054	8.134	9.996	1.359
Large	Total(200)	11.100	7.200	8.719	0.662	12.936	5.978	8.853	1.229
	Train Set(140)	11.100	7.200	8.790	0.726	12.936	5.978	9.140	1.266
	Val Set(20)	9.200	7.800	8.500	0.407	9.996	7.305	8.345	0.708
	Test Set(40)	9.000	7.200	8.455	0.478	10.192	7.056	8.102	0.858

Table 2. R^2 and MSE of estimated SSC for each model

Sample Size	Model	preprocessed	Second-order differential		MSC	
			R^2	MSE	R^2	MSE
Small(50)	SVR	✓	0.104	0.116	0.089	0.123
	KNNR	✓	0.362	0.083	0.289	0.096
	AdaBoost	✓	0.536	0.060	0.502	0.068
	PLSR	✓	0.557	0.055	0.528	0.062
	Con1dResNet	Original data	0.498	0.065	-	-
Large(200)	SVR	✓	0.078	0.205	0.075	0.207
	KNNR	✓	0.337	0.147	0.316	0.152
	AdaBoost	✓	0.609	0.089	0.581	0.096
	PLSR	✓	0.713	0.064	0.710	0.067
	Con1dResNet	Original data	0.901	0.018	-	-

Table 3. R^2 and MSE of estimated SSC for each model with all sample

Model	preprocessed	Second-order differential		MSC	
		R^2	MSE	R^2	MSE
SVR	✓	-0.037	1.108	-0.054	1.116
KNNR	✓	-0.329	1.251	-0.456	1.318
AdaBoost	✓	0.217	0.694	0.261	0.675
PLSR	✓	0.384	0.552	0.398	0.548
Con1dResNet	Original data	0.532	0.416	-	-